Laser Doppler Velocimetry Characterization of Unsteady Vaned Diffuser Flow in a Centrifugal Compressor

William J. Gooding[1]
School of Mechanical Engineering,
Purdue University,
West Lafayette, IN 47906-1757
e-mail: wgooding@purdue.edu

John C. Fabian
School of Mechanical Engineering,
Purdue University,
West Lafayette, IN 47904
e-mail: jcsfabian@gmail.com

Nicole L. Key
School of Mechanical Engineering,
Purdue University,
West Lafayette, IN 47907
e-mail: nkey@purdue.edu

Modern turbomachinery faces increased performance demands in terms of efficiency, compactness, and pressure-rise. Advancements in computational technology have allowed numerical methods to become the backbone of design development efforts. However, the unique complexities of centrifugal compressor flow-fields pose difficult computational problems. As such, advanced experimental methods must be used to obtain high-quality data sets to further inform, improve, and validate computational methods in complex flow regimes. A recent experimental work on a high-speed centrifugal compressor has provided detailed, unsteady, three-component velocity data using laser Doppler velocimetry. A passage vortex is present, and its nascent tied to the increased incidence at mid-span associated with impeller wake flow. This vortex begins in the hub-pressure side corner and grows to fill the passage and become temporally stable. The vortex development is unsteady in nature, and the unsteady effects persist 40% downstream of the throat. Distinct jet and wake flow patterns from the impeller also do not agglomerate until 40% downstream of the throat. Additionally, the critical impact of the unsteady flow development on the time-averaged flow-field is explained. [DOI: 10.1115/1.4046230]

Keywords: centrifugal compressors and pumps, measurement techniques

Introduction

The rapid advancement of gas turbine engine technology since the 1940s has occurred due to a tandem investment in modeling and experimental development. Early design efforts relied almost exclusively upon conventional experimental studies and design correlations as the complexity of the flow-fields inherent to turbomachinery was far beyond contemporary computational resources. Modern advances in computing technology have greatly increased the reliance upon numerical methods in the design phase. Experimental studies are crucial for validating models, especially in flow regions where numerical methods are known to fall short.

Modeling flow through centrifugal compressors is challenging since strong adverse pressure gradients, significant streamline curvature, system rotation, large-amplitude unsteady fluctuations, and significant secondary flows are all intrinsic to these machines. Each of these factors in isolation is known to cause errors in most current turbulence closure methods [1]. This motivates a need for additional experimental data to inform, improve, and validate computational methods. Accurate and predictive methods are imperative as designs progress toward smaller passages, higher pressure ratios, and novel design spaces.

With modern design trends toward engines with smaller cores to obtain higher bypass ratios, conventional measurement techniques in these types of machines pose even more significant disadvantages. Smaller passages mean more dramatic blockage effects of intrusive probes [2,3] and more drastic property gradients (with associated measurement errors). Steady probes can also have significant errors in the regions of strong fluctuations [2]. These factors limit the usefulness of conventional techniques in furthering the present understanding of centrifugal compressor internal flow physics that is critical to improving numerical methods and informing more efficient and novel designs. Alternative methods—less intrusive and more capable of capturing complex flow structures—are vital to reaching the lofty design goals of the next decades. Eckardt claims that the benefits of detailed, unsteady, non-intrusive experimental studies at real operating conditions are twofold: they will develop a more detailed physical understanding of the internal flow phenomena, and will accelerate the development of computational fluid dynamics models to push the performance of turbomachinery further toward its "ultimate gains [2]." Various high-speed experimental studies have concluded that computational methods are, generally, too dissipative [4], do not match with experimentally observed diffuser flow progressions [5], and lack detailed data sets for validation [4–6]

The non-intrusive technique utilized in this study, laser Doppler velocimetry (LDV), was first developed by Yeh and Cummins in 1964 [7]. When compared to particle image velocimetry, LDV allows easier three-component measurements and reduced need for optical access. Compared to Laser-2-Focus and other time-of-flight methods, LDV allows simultaneous measurements of multiple velocity components and higher data rates [8,9].

Laser Doppler Velocimetry and Laser-2-Focus have been utilized extensively on centrifugal compressors. Two canonical studies by Eckardt [10,11] and Krain [12,13] used Laser-2-Focus to measure, in series, two components of the velocity vector field through the impeller. These provided the first direct measurement of Dean's jet-wake structure and elucidated the development of impeller flow patterns. Eckardt used a 5×9 measurement grid at the impeller trailing edge to observe the impeller wake location and shape [11]. Krain used a 5×6 measurement grid in the diffuser inlet region to observe unsteady effects and the dissipation of the jet-wake flow upstream of the passage [12]. LDV was first utilized in one- or two-component configurations on low-speed machines [14–16]. On high-speed machines, data were first obtained by Skoch et al. at the National Aeronautics and Space Administration (NASA) [17]. Three separate one-component measurements, taken at different probe orientations, were phase-locked and combined to provide two-component results. These data demonstrated a linear velocity gradient across the impeller passage at the trailing edge, similar to Ref. [13], which decayed rapidly through the vaneless diffuser.

[1]Corresponding author.

Contributed by the International Gas Turbine Institute (IGTI) of ASME for publication in the Journal of Turbomachinery. Manuscript received June 26, 2019; final manuscript received January 6, 2020; published online February 5, 2020. Assoc. Editor: David G. Bogard.

Stahlecker and coauthors [18,19] obtained the first high-speed LDV data in a compressor with a modern, vaned diffuser. Repeated two-component measurements were ensemble-averaged and combined to yield the three-component flow field. The results indicated the presence of a large passage vortex through the vane passage. This vortex developed from a strong suction-to-pressure side shear flow near the shroud beginning in the semi-vaneless space, resulting in a temporally stationary vortex.

More recently, Schleer and Abhari obtained a limited amount of true three-component LDV data in the inlet region of the vaneless diffuser of a turbocharger. They observed a significant change in the secondary flow pattern at the impeller exit with a large change in tip clearance [20].

The data presented here represent, to the authors' knowledge, the first unsteady, three-dimensional, and simultaneous three-component velocity data obtained within a modern centrifugal compressor with a vaned diffuser using non-intrusive measurement techniques. Other detailed LDV studies have been conducted [4–6], typically constructing the three-component flow-field from multiple tests, conducted in series, each obtaining one or two components. This study illustrates the importance of resolving the spanwise flow component simultaneously to better capture the development of secondary flow structures. Additionally, this study utilizes a machine with a smaller radius ratio (1.08) than many of the previous works, more representative of modern designs for aeroengine applications.

Test Compressor

The single-stage centrifugal compressor with vaned diffuser is given in Fig. 1. The test facility capabilities, geometric details, and baseline performance data are given in Ref. [21]. The design rotational speed of the impeller is 22,500 rpm, and it operates at engine-representative Mach numbers. The backswept impeller has 15 full blades and 15 splitter blades that begin at 34% of the meridional passage. The diffuser has 35 thin vanes beginning at a radius ratio of 1.08. From the baseline geometry, a second shroud was manufactured, and the diffuser cover plate modified to allow optical access to nearly 85% of the impeller and diffuser flow-fields. In the diffuser, optical access extends to approximately 80% of the diffuser vane passage.

The compressor maps in terms of pressure ratio and efficiency acquired with both configurations, the LDV shroud and the baseline shroud, are depicted in Fig. 2. The symbols represent stable operating points at which the full performance data were obtained. The experimental surge point, which remained unchanged between the two configurations, is marked along with the point at which

Fig. 1 Test compressor cross section

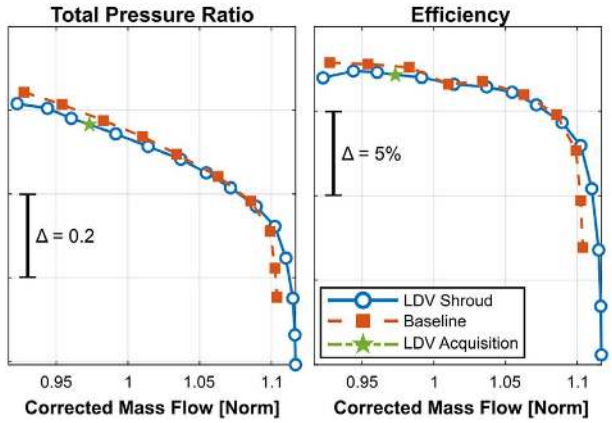

Fig. 2 Baseline and LDV shrouds' overall performance comparison

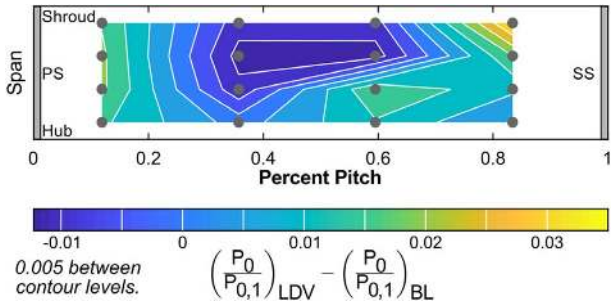

Fig. 3 Difference in diffuser exit total-pressure measurements between the LDV and baseline configurations

the LDV data were acquired. An abradable coating is applied to the flow path surface of both shrouds and slight differences in the application of this coating were unavoidable due to manufacturing limitations. The resulting small differences in the flow path contour are responsible for the minor differences in the overall performance: most notably, the 1% difference in the choking mass flow.

Four-element total-pressure rakes are located at the exit of the diffuser passage. Eight rakes, two at each of four pitchwise positions, are distributed around the circumference of the diffuser. The difference in the diffuser exit total-pressure measurements, P_0, normalized by the impeller inlet total pressure, $P_{0,1}$, between the configurations is given in Fig. 3, plotted on a single diffuser passage at the LDV acquisition point (as indicated in Fig. 2). The gray circles indicate the measurement locations, and the position of the vanes is depicted in gray with the pressure surface (PS) on the left and the suction surface (SS) on the right. The average difference in these measurements is 0.01, which is less than 0.5% of the overall total-pressure rise of the stage. These data support the conclusion that the modifications made to the compressor geometry to allow optical access did not significantly alter the flow field being observed.

The performance data were corrected to sea-level standard, accounting for humidity effects, while updating calculations real-time during tests. The operating condition for all velocity data, acquired over four months, was maintained within ±0.075% in terms of corrected speed and ±0.55% in terms of the ratio of pressure ratio to corrected mass flow. All velocity data were corrected to sea-level standard conditions.

Laser Doppler Velocimetry System

The LDV system used in this study is a commercially available three-component system from Dantec Dynamics. An in situ developed seed traverse system and TSI 9306 six-jet atomizer were used

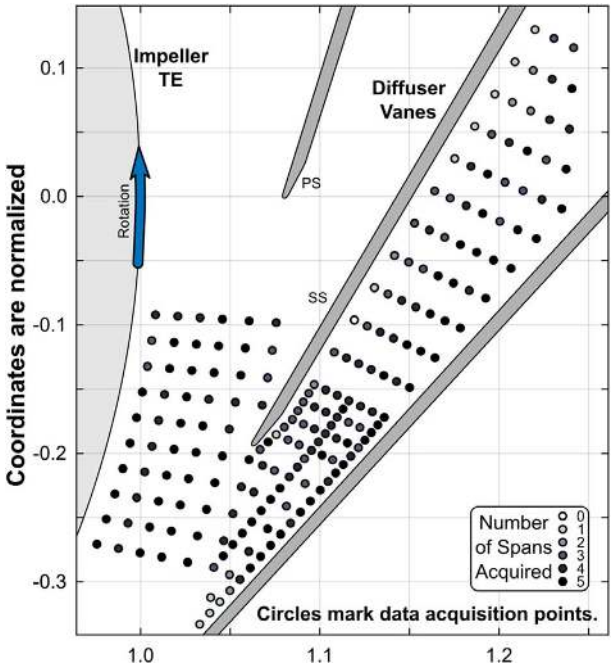

Fig. 4 Initial test matrix

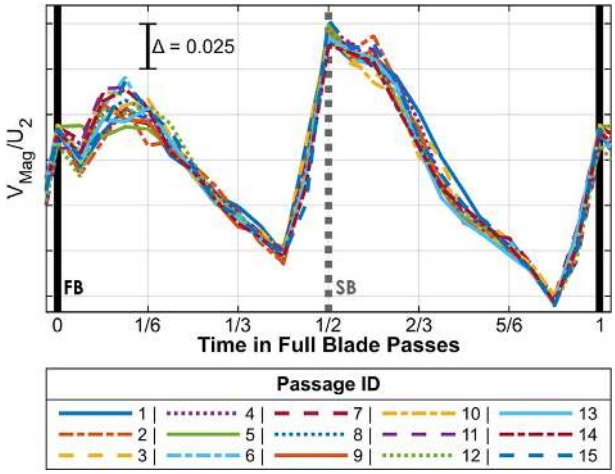

Fig. 5 Passage-to-passage variation in velocity magnitude at Point 44

to produce an aerosol of di-ethyl-hexyl-sebacate. The output from a 5.0 Watt Argon-Ion laser head (Coherent Inc.) is split, and one beam is passed through a Bragg cell to produce a 40-MHz frequency shift. The three primary bands (514.5 nm, 488.0 nm, and 476.5 nm) of these two beams are then selected and passed via fiber optic cables to the probe heads. One probe head outputs two beam pairs while a second outputs the third beam pair to resolve the third velocity component. The two-component probe is mounted in a rotatable support while the one-component probe's mount can pan, tilt, and shift axially. Both probes are mounted to a three-axis traverse system with a range of 24 in (610 mm) and a resolution of 0.00025 in (6.25 μm). Once fixed to the traverse, the probes are aligned, utilizing the probe supports' degrees-of-freedom, to pass through a 0.002-in. (50 μm) diameter pinhole to ensure measurements are obtained at a single point in space. Further details regarding the LDV system, special steps taken to increase the data rate, and data processing techniques are given in Ref. [22]. The uncertainty analysis procedure given in Ref. [23], applied to these data, yields a typical uncertainty of less than ±1% in the streamwise and pitchwise velocities, ±2% in the spanwise velocity, and ±1 deg in the flow angle. In regions of separated flow and adjacent to walls, where the signal-to-noise ratio decreases, these values can triple.

Currently, data at 780 points out of the initial test matrix of 1000 points through the diffuser passage (as marked in Fig. 4) have been obtained with the compressor operating at design conditions. Data acquisition was attempted at each of the locations marked in Fig. 4 at 15%, 30%, 50%, 70%, and 85% span. The tone of the circles indicates the number of spanwise positions at which data have been acquired. These data will form the first phase of an ongoing study which will continue to further resolve spanwise gradients and obtain the Reynolds stress measurements at key locations. Results will be utilized to validate and buttress turbulence closure models in the specific and unique application of centrifugal compressors.

Data Processing

Velocity data are ensemble-averaged into a single full-blade and splitter-blade dual passage using a once-per-revolution signal and assuming all fifteen dual passages are identical. To justify this assumption, the velocity magnitude data at the impeller trailing edge for all fifteen dual passages are plotted in Fig. 5. The horizontal axis is time, measured relative to a full-blade passing event, the vertical axis is the velocity magnitude, normalized by the impeller tip speed U_2 and the positions of the full and splitter blades are indicated by the solid and dashed lines, respectively. The average of the difference between the maximum value and the minimum value from all fifteen passages is less than 2.5%, a value which is partially inflated by the sharp gradients measured behind each blade. The impeller angular position at each velocity sample is rounded to the nearest 1 deg, yielding 24 time increments per full-blade passing event. At this point, a mixture-model-based noise isolation algorithm, developed in situ, is applied. Invalid signals arising from reflections were present in a portion of the data at 40 MHz and 132 MHz (corresponding to zero velocity and approximately 620 ft/s (190 m/s)). This algorithmic method effectively and efficiently isolates and removes these erroneous measurements from the data sets. The development and validation of this method is

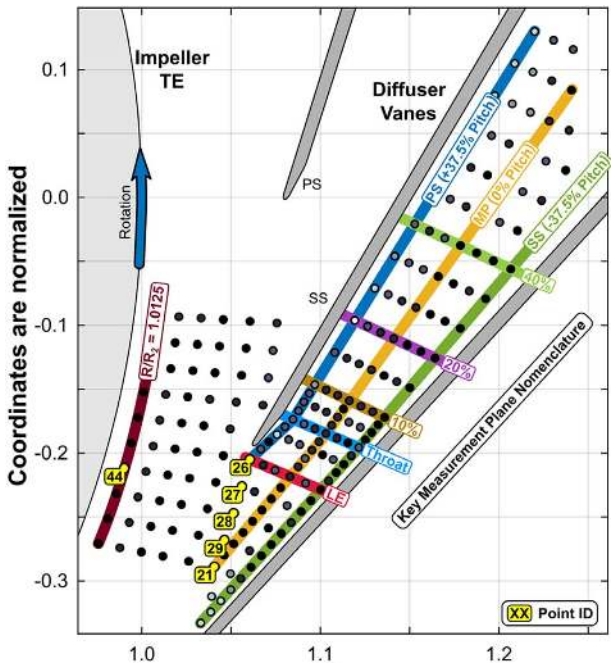

Fig. 6 Key measurement locations

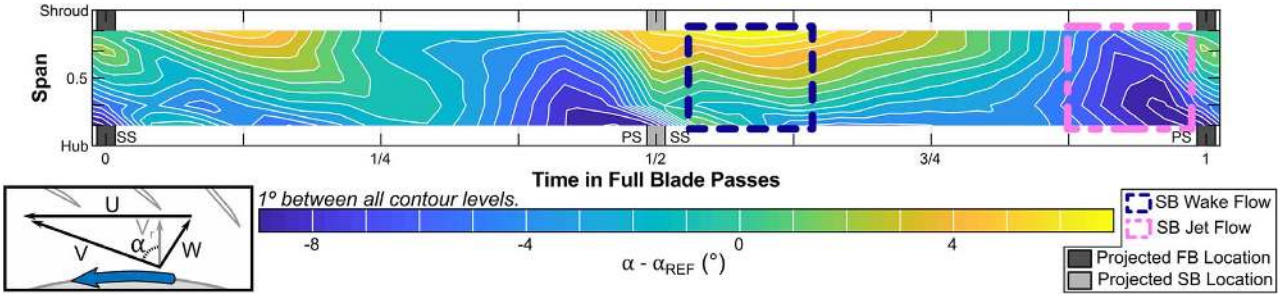

Fig. 7 Flow angle difference from reference (*REF*) value at Point 44 ($R/R_2 = 1.0125$)

given in Ref. [22]. Each time increment is then transformed from the measurement, skew coordinate system to the laboratory, orthogonal system. The time average is computed as the mean of the ensemble average from each time increment.

Vector data are also analyzed in the passage coordinate system. The streamwise direction, in the vaneless space and semi-vaneless space, is defined as tangent to the logarithmic spiral aligning with the vane leading edge. Within the passage, the streamwise direction is parallel to the passage centerline. The positive streamwise sense is in the direction of the primary flow. The pitchwise direction is defined as perpendicular to the streamwise direction in the plane of Fig. 4 with the positive sense defined as toward the pressure side of the vane. Mid-passage (MP) is defined as 0% pitch with the pressure and suction surfaces (PS and SS) being at +50% and −50%, respectively. Obtaining a right-handed coordinate system stipulates the spanwise direction as being directed perpendicular to the plane of Fig. 4 with the positive sense being from the hub toward the shroud (out of the page). The critical measurement planes at which results will be discussed are highlighted and notated in Fig. 6.

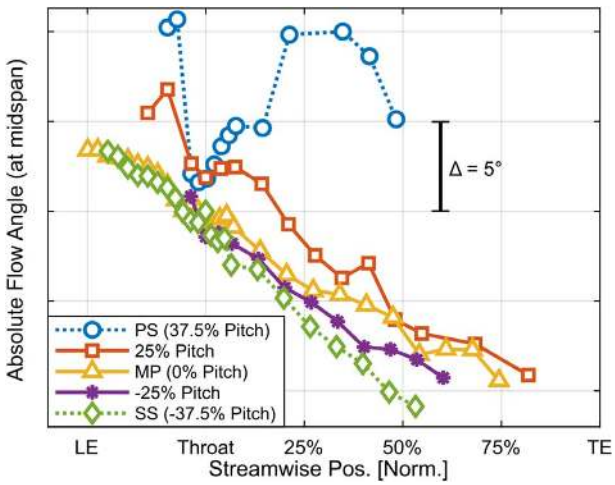

Fig. 8 Time-averaged flow angle at 50% span

Experimental Results

This study focuses on the diffuser flow field. From that perspective, the impeller outlet flow conditions form an inlet boundary condition for this work. The absolute-frame flow angle experimental data are given in Fig. 7 at Point 44, 1.25% downstream of the impeller tip (that is, at a radius ratio, R/R_2, of 1.0125%). Two impeller passages are presented between two full blades (on the left and the right of the graph) with a splitter blade in the middle, as labelled. The horizontal axis is time, measured relative to a single full-blade passing event. This figure illustrates the complex nature of the diffuser inlet flow field. Within each passage, hub-to-shroud flow angle gradients of 14 deg are measured at a single instant in time and cross-pitch gradients of 15 deg are measured at a single span. The wake, adjacent to the suction surface, is characterized by more tangential flow (positive values of α–α_{REF}) while the jet, adjacent to the pressure surface, is characterized by more radial flow (negative values of α–α_{REF}). This generality applies to both passages; however, the shape, location, and magnitude of the wake flow differ between the two passages depicted. The wake and jet trailing the splitter blade, marked on the figure, are tracked downstream in the subsequent discussion.

The velocity results within the diffuser passage show that a region of flow separation develops along the pressure surface of the diffuser vane. This is evident in the flow angle progression through the passage along constant-pitch lines at mid-span (Fig. 8). Across most of the passage, the vanes effectively turn the flow. However, along the pressure side, the flow angle does not continue to decrease downstream of the throat as separation has occurred and the flow is not adequately following the vane trajectory.

This difference can be linked to the downstream propagation of the unsteady incidence field arising from the jet-wake impeller discharge flow. To determine the instant in time at which the impeller jet and wake pass the leading edge of the diffuser, the convection of the impeller discharge flow pattern through the vaneless space was tracked. Figure 9 depicts the unsteady variation in the flow angle, at mid-span, through the vaneless space and into the semi-vaneless space at a constant circumferential position. The horizontal axis is time, measured relative to a full-blade passing event. The data from

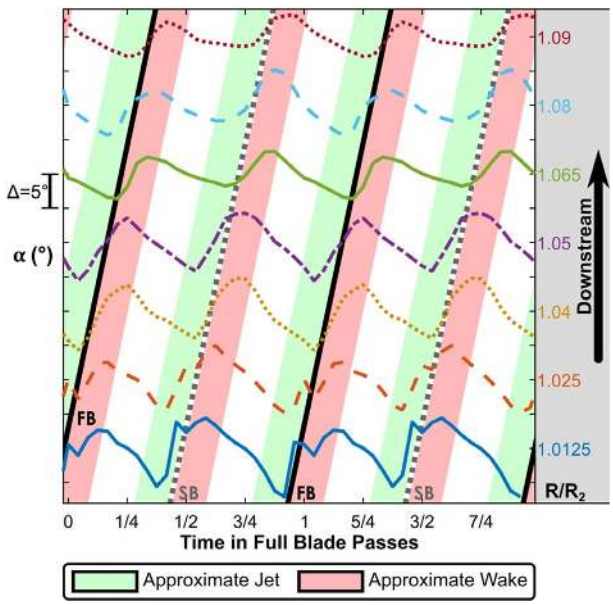

Fig. 9 Flow angle progression showing jet and wake convection through the vaneless and semi-vaneless space

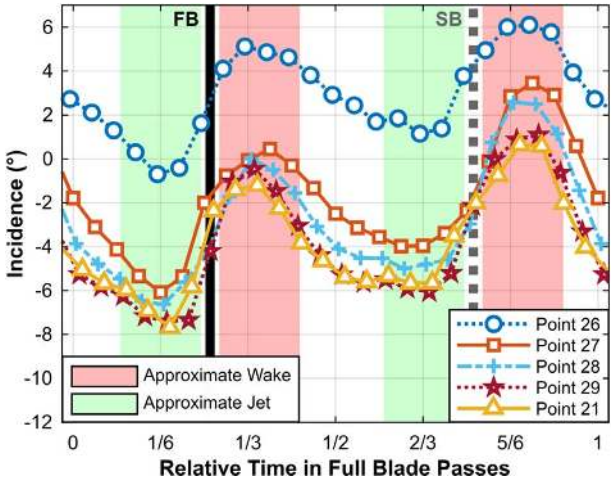

Fig. 10 Leading-edge incidence at 50% span

each geometric position are offset on the vertical axis to better illustrate the propagation of the impeller exit discharge flow. The approximate temporal projection of the full blades (solid lines), splitter blades (dashed lines), jet flow (shaded regions to the left of the blades), and wake flow (shaded regions to the right of the blades) are tracked downstream by matching the sharp increase in flow angle that occurs with each blade passage.

The incidence is defined as the local flow angle (defined from the radial direction) minus the vane setting angle at the leading edge. Figure 10 presents the unsteady incidence at five points along the diffuser vane leading edge radius ($R/R_2 = 1.08$) at mid-span (Fig. 6 illustrates the geometric locations of points). The horizontal axis is the *relative* time, measured relative to a full-blade passing event aligned with that particular point. The temporal data from each point were offset by the circumferential position of the point to yield this *relative* time. This results in the approximate positions of the jet and wake flow being aligned, whereas they would be offset if the horizontal axis were absolute time. The figure depicts the passage of one full blade and one splitter blade and, due to the ensemble averaging procedure, repeats cyclically—a relative time of 0 and 1 is synonymous.

The wake passage is indicated by the two distinct peaks in the flow angle and is highlighted to the right of each blade. The wake that developed along the suction side of the full blade corresponds to the peak centered around a relative time of 1/3, while the splitter-blade wake is indicated by the peak centered around 5/6. This graph illustrates that the wake flow, especially following the splitter blade, is characterized by a significantly more positive incidence than the other time periods in a blade passage event. At the radius associated with the diffuser leading edge, the vane acts to divide the incident flow between the clockwise and counterclockwise diffuser passages. Regions of positive incidence indicate flow diverted toward the counterclockwise passage while regions of negative incidence indicate flow tending to enter into the passage being studied. At Point 26, immediately upstream of the vane leading edge, the flow is diverted into the adjacent, counterclockwise passage at nearly all time-steps. Additionally, the other points in the graph indicate that during the splitter-blade wake passage—and only during the splitter-blade wake passage—flow follows a path toward the adjacent passage as far as the passage centerline (Point 21). The data at other spanwise positions reveal that this behavior is most pronounced at mid-span. Qualitatively, this pattern can be described as follows: the wake flow causes an intermittent "jumping" of flow into the adjacent passage at mid-span which is more pronounced within the splitter-blade wake. As will be demonstrated, this has a significant impact on the secondary flow development in the passage.

The more severe nature of the wake trailing the splitter blade is contrary to what is expected. Krain showed that the wake trailing the full blades was more severe due to the longer flow path and increased boundary layer development [12]. However, Ahmed and Elder [24] showed that the positioning of the splitter leading edge in terms of pitchwise location and leading-edge angle can lead to different behavior on either sides of the splitter blade. It is likely that positive incidence at the splitter leading edge leads to a stronger adverse pressure gradient, more rapid boundary layer growth, and a more severe wake along the splitter suction surface. Future LDV measurements within the impeller will be able to verify this hypothesis.

Wake Convection. The convection of wake flow through the diffuser passage and the propagation of the unsteady incidence field is given in Fig. 11. The corresponding figure for the convection of jet flow through the diffuser passage is depicted in Fig. 12. These figures track the flow from the wake and jet trailing the splitter

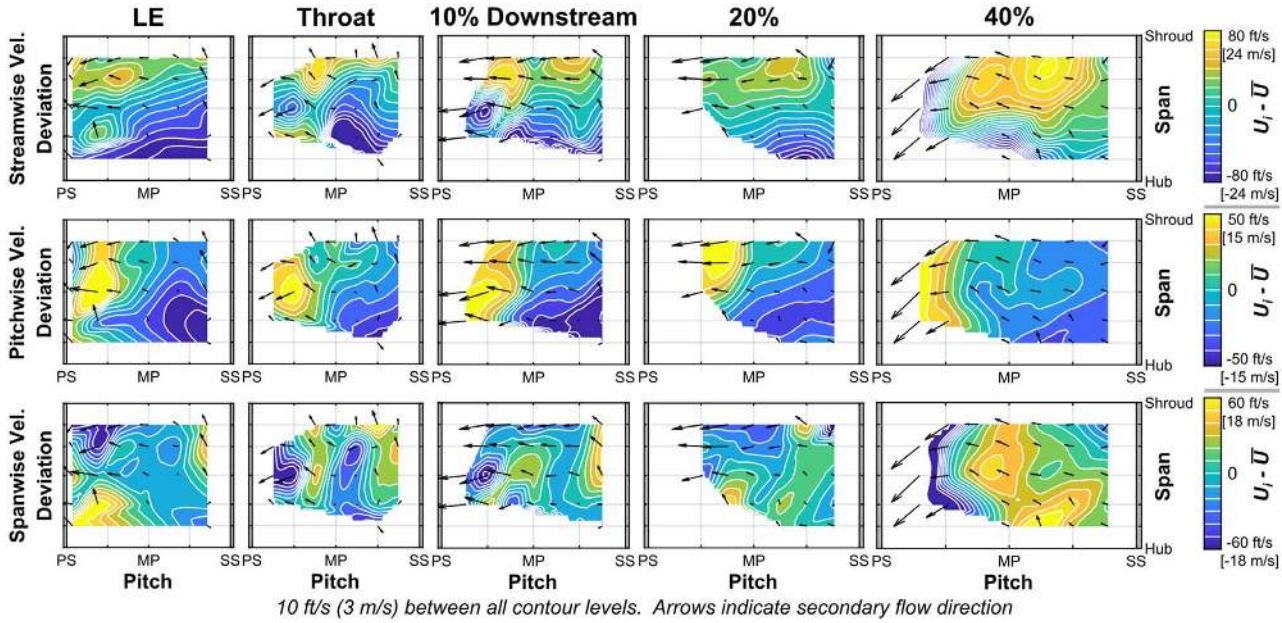

Fig. 11 Deviation of each velocity component from the instantaneous planar mean value ($\overline{U}$) during wake propagation

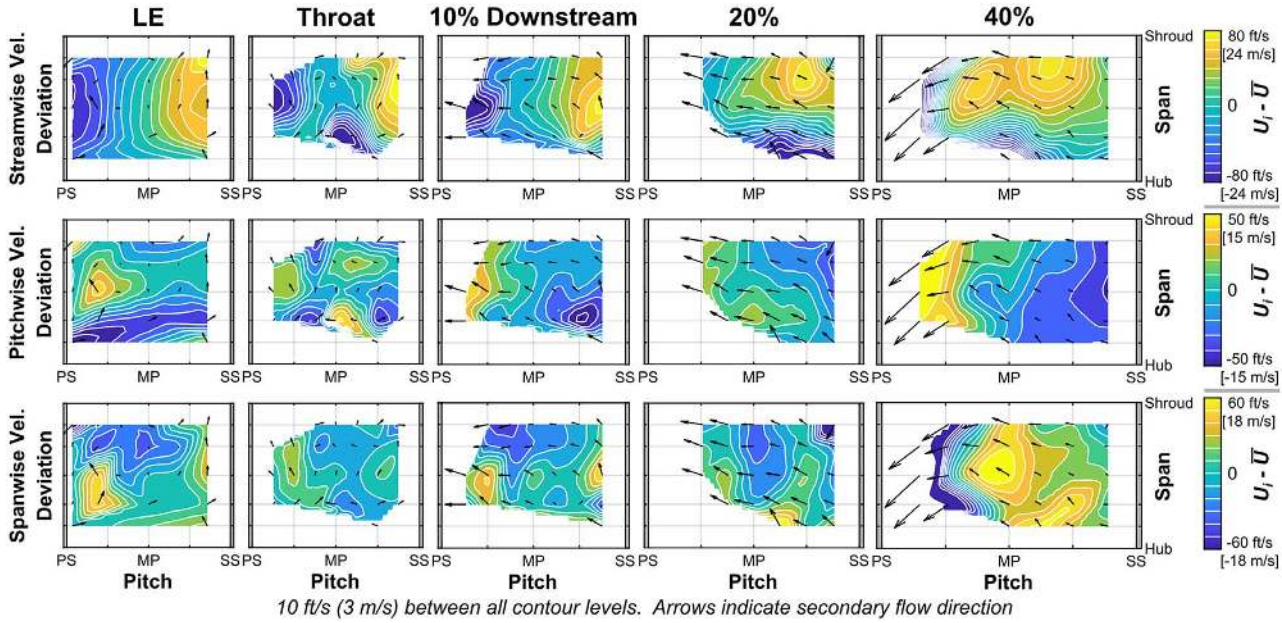

Fig. 12 Deviation of each velocity component from the instantaneous planar mean value ($\overline{U}$) during jet propagation

blade, as marked in Fig. 7, as it propagates through the diffuser. The wake and jet trailing the full blade show identical patterns that are slightly less distinct, due to the reduced leading edge incidence. In these figures, the three components of velocity are presented across the rows: streamwise on the top, pitchwise in the middle, and spanwise on the bottom. Within each plot, the velocity component data are presented as the difference between individual measurements, U_i, from the mean of all measurements of that component across the plane of interest at that instant in time. This was done to allow a consistent and physically meaningful color scale to be used across each component. These data are reported at the cross-passage planes defined in Fig. 6 at all spans, beginning at the most upstream plane and proceeding downstream from the left to the right. Each plane is plotted at a single, distinct snapshot in time, chosen to correspond to the wake (or jet) passage through that plane.

Convection plots (similar to Fig. 9) were used along the passage centerline to determine the snapshot in time that was most representative of wake (or jet) flow through each plane. The diffuser pitch is less than the impeller pitch, meaning that the spatial extent of the wake (or jet) covers nearly the full diffuser passage at the leading edge. The passage-bounding vanes are depicted on either sides of the graphs, with the pressure surface (PS) on the left and the suction surface (SS) on the right. The color scales for each component are given on the far right, and the contour levels are separated by 10 ft/s (3 m/s) in all cases. The arrows overlaid on the contours indicate the secondary flow direction and magnitude at measurement locations. The following discussion of the wake and jet convection and the data presented in Figs. 11 and 12 are summarized graphically in Fig. 13.

At the leading edge (LE) plane (in the semi-vaneless space, presented in the first column of Fig. 11), the high incidence at the leading edge at mid-span observed in Fig. 10 is illustrated in both the secondary flow direction and the high pitchwise velocity. An important companion is evident in the spanwise velocity graph. A lobe of high, positive (toward shroud) spanwise velocity is present adjacent to the hub with an opposite lobe of high, negative (toward the hub) spanwise velocity adjacent to the shroud, observable in the first column, the third row of Fig. 11. The endwall flow is drawn up into the mid-span to "replace," so to speak, the high-incidence flow that passes into the adjacent passage. More fundamentally, the strong spanwise gradient in the pitchwise velocity developed as the wake flow impacts the leading edge contributes to the production of streamwise vorticity. This pattern forms the beginnings of a vortex along the pressure surface of the vane in the hub corner.

Tracking downstream, this hub-pressure side vortex is discernible at the throat (presented in the second column of Fig. 11). The counterclockwise vortex has grown in the spanwise direction, to cover the full span, and in the pitchwise direction to nearly mid-passage. This vortex is most evident in the vertical band of negative spanwise velocity along the pressure side immediately adjacent to a vertical band of positive spanwise velocity present in the second column, the third row of Fig. 11. Although no data have been obtained in the hub-pressure side corner at the throat, the pitchwise velocity data indicate that the vortex center is located closer to the hub of the passage.

Approximately 10% downstream of the throat (100% being the vane trailing edge), the vortex has grown further and flattened across the passage. Most of the secondary flow behavior is in the pitchwise direction, toward the pressure side. Along the suction side, a strong positive spanwise velocity reveals the counterclockwise nature of the now full-passage vortex. A nearly identical pattern is present at 20% downstream of the throat (the fourth column of Fig. 11). There are two discernable differences between 10% and 20% downstream planes. First, a region of slight positive spanwise velocity exists along the hub surface, between mid-passage and the suction surface. Second, the high-streamwise velocity region adjacent to the shroud is more consistent in the pitchwise direction and the overall plane gradient in the streamwise velocity is more strictly in the spanwise direction.

Finally, at approximately 40% downstream of the throat, a vortical structure is present spanning the entire passage. The bulk motion is toward the shroud adjacent to the suction surface and also adjacent to the hub, between mid-passage and the suction surface. Closer to the pressure side, the vortex drives the flow down toward the hub. A distinct region of high-streamwise velocity is present near the shroud representative of a low-loss region. A graphical summary of this discussion of the wake flow development through the diffuser is given in the top row of Fig. 13.

Jet Convection. The corresponding data for the jet convection through the diffuser passage are presented in Fig. 12. A comparison

between the jet and the wake progression contours highlights the difference between the flow development through the diffuser between the jet and the wake and evinces the extent to which unsteady structures persist in the passage. At the LE plane (in the semi-vaneless space, presented in the first column of Fig. 12), the jet flow exhibits a gradient of increasing streamwise velocity from the pressure side to the suction side. The other velocity components do not demonstrate coherent structures as were present in the wake flow. Similar behavior is observed at the throat (presented in the second column of Fig. 12). The secondary flow magnitude is relatively low, as indicated by the short arrows overlaid on the contour, and no coherent pattern is discernable in the secondary flow vectors. The most evident feature is in the streamwise velocity where the high-velocity region adjacent to the suction surface at the LE plane has grown more distinct.

A coherent secondary flow structure first begins to appear 10% downstream of the throat (the third column of Fig. 12). The secondary flow tends to be toward the shroud along the suction surface. Across the rest of the passage, the secondary flow is directed toward the pressure side. A clear vortical structure is not discernible, especially when considering the chaotic spanwise velocity contour. The high-streamwise velocity region noted earlier is still present and adjacent to the suction surface of the vane.

Further downstream, (20% downstream of the throat, the fourth column of Fig. 12), the overall secondary flow structure is beginning to mirror the structure observed through the wake passage. The bulk motion is consistently up (toward the shroud) and across the passage (toward the pressure side). Details are still different between the wake flow, presented previously, and the jet flow. Namely, the jet flow has a stronger and more consistent positive (toward shroud) spanwise velocity component across the full passage. The result is a secondary flow direction toward the shroud-pressure side corner of the passage that is relatively constant across much of the passage. The high-streamwise velocity flow adjacent to the suction surface has begun to shift toward the shroud and spread across the passage.

By the final plane presented here, 40% downstream of the throat, the secondary and primary flow structures observed in the jet and the wake flow are nearly indistinguishable. A high-streamwise "core" flow is present adjacent to the shroud and focused closer to the suction side of the vane. Through the wake passage, this core flow was first observed at the Throat. Within the jet flow, however, this core began further upstream and remained adjacent to the suction surface. The vortical structure that developed acted to convect this core flow toward the shroud and across the passage.

Unsteady Nature of Passage Vortex. The temporal behavior of the described passage vortex is indicated in these figures, and a cartoon summarizing the unsteady nature of the vortex development is given in Fig. 13. Previous studies have concluded that unsteady fluctuations are effectively dissipated upstream of the throat. Additionally, Stahlecker et al. [19] concluded that this passage vortex formed upstream of the throat and was temporally steady. These results support a different conclusion. Wake flow, at impeller discharge, is characterized by a higher velocity magnitude in the absolute frame (the "wake" refers to the velocity deficit in the *relative* frame). This translates to a higher streamwise velocity within the diffuser passage of the flow that originally formed the impeller wake. From a Lagrangian perspective, fluid particles that originally formed the impeller wake will convect forward into the preceding jet flow, causing the wake region to grow until the jet and wake flow are indistinguishable. From the Eulerian perspective, this results in a temporal broadening of flow structures associated with the wake flow. This is reflected in the contours given in Figs. 11 and 12 as the jet flow grows to emulate the wake flow, in terms of both primary and secondary flow structure, as the flow propagates downstream. What is typically referred to as "wake dissipation" is perhaps better described as an agglomeration of the jet and wake flow as they merge to form a single, coherent flow structure. From the figures, it is evident that two distinct flow patterns are still present 10% downstream of the throat. At 20% downstream, the jet secondary flow pattern is beginning to resemble the wake secondary flow pattern; however, the primary flow patterns are still easily distinguishable. It is not until 40% downstream of the throat that the jet and wake have fully agglomerated in both primary and secondary flow structures.

Impact on the Steady Flow Field

The time-averaged flow angle data (Fig. 8) indicate a significant flow separation along the pressure surface of the vane. However, the high positive incidence at the vane leading edge (Fig. 10) would, intuitively, promote separation along the *suction* surface. This apparent discrepancy may be explained by the unsteady vortex development as demonstrated experimentally. The spanwise gradient in incidence induces a streamwise vortex at the leading edge along the pressure side of the vane. This vortex, initially, acts to drive low-momentum endwall flow toward mid-span. Simultaneously, a strong adverse pressure gradient is present around the vane leading edge as the flow adjusts to the presence of the vanes. This low-momentum flow exacerbates the boundary layer that is already prone to separation. Upstream of the throat, the growing vortex present in the wake flow keeps low-momentum flow entrained along the pressure side, prevents higher-momentum core flow from re-energizing the boundary layer, and increases the propensity of the flow to separate. At the same time, the strong

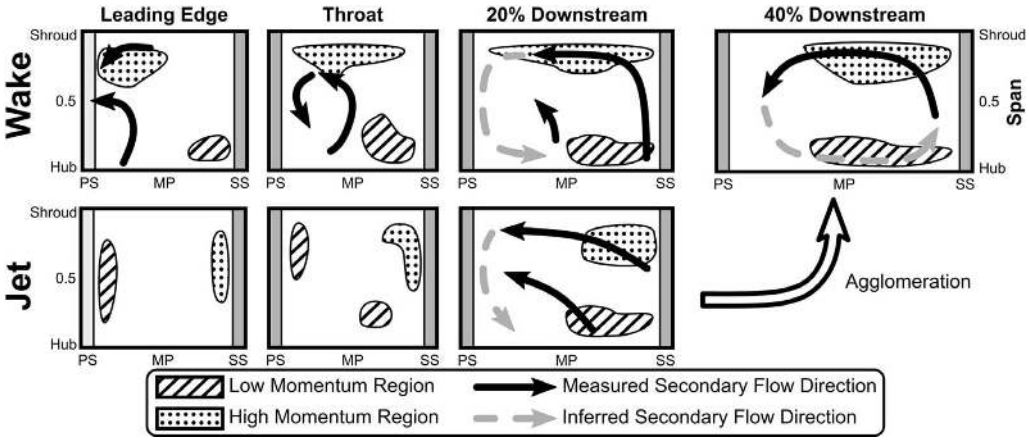

Fig. 13 Summary of the unsteady nature of the passage vortex

toward-pressure side pitchwise velocity that develops acts to entrain the lower-momentum flow adjacent to the hub into the hub-pressure side corner. In the measurements, this flow separation is indicated by regions where data were not easily obtained. Few seed particles are able to penetrate regions of separated or recirculating flow resulting in prohibitively low data rates. Future work on seed introduction and involving longer test times will address this issue. Once fully developed—to span the full passage and become temporally steady—the vortex acts to feed the high-momentum core flow into the region of separated flow. This allows the boundary layer to reattach toward the trailing edge of the vane and prevent significant performance detriments from occurring.

The nature of this boundary layer separation is not properly explained by a steady interpretation of the passage vortex. If the flow structures are assumed to be steady, then the vortex would feed the high-momentum core flow adjacent to the shroud into the hub-pressure side corner. This would reenergize and stabilize the boundary layer along the pressure surface of the vane. The separation would likely occur on the suction surface of the vane as would follow from the incidence data presented in Fig. 10. Only the unsteady development of the passage vortex adequately explains the observed steady flow-field with separation occurring along the pressure surface of the vane.

Conclusions

The data presented reveal the unsteady, three-component velocity field within a modern centrifugal compressor vaned diffuser obtained using a non-intrusive technique. Velocity data indicate the presence of a time-averaged region of boundary layer separation along the pressure surface of the vane. These data also exhibit the unsteady nature of the development of a passage vortex in the vane passage. At the vane leading edge, the high incidence at mid-span that exists when the impeller wake impinges on the leading edge acts to draw endwall flow toward mid-span. This action forms a vortex which grows, both in space and in time, as it propagates downstream. Distinct jet and wake flow structures are present 20% downstream of the throat, before the wake-associated passage vortex becomes the dominant secondary flow feature. It is not until 40% downstream of the throat that unsteady features are fully dissipated in terms of both secondary and primary flow characteristics. The unsteady development of this passage vortex also appears to have a significant impact on the steady performance of the diffuser and helps explain the pressure-side region of flow separation.

These data have informed regions that would benefit from additional study. Specifically, further work will be focused on obtaining a higher geometric resolution to better identify vortical structures in the passage. This will include data at a greater number of distinct spanwise locations to improve the resolution of hub-to-shroud gradients and additional data in regions of potential flow separation. Additionally, coincident data with long collection times will be obtained at a subset of geometric points to directly measure the Reynolds stress field and its development at key locations in the diffuser. Finally, these data will be utilized to motivate possible improvements in modeling parameters and best-practices.

Acknowledgment

The authors thank the Rolls-Royce Corporation for its funding and permission to publish this work. Additionally, Matt Meier, Grant Malicoat, and Ruben Adkins-Rieck's work on the research team throughout this project is much appreciated. Finally, the technical expertise of Cliff Weissman from Dantec Dynamics was crucial to the success of this study.

Nomenclature

$\overline{U}$ = instantaneous mean velocity for plane
U_i = particular measurement of velocity component i
U_2 = impeller tip speed
P_0 = total pressure
$P_{0,1}$ = impeller inlet total pressure
FB = full blade
MP = mid-passage
PS = pressure side
R/R_2 = radius ratio (relative to the impeller tip radius)
SB = splitter blade
SS = suction side
α = absolute flow angle

References

[1] Wilcox, D., 2006, *Turbulence Modeling for CFD*, DCW Industries, Inc, La Canada, CA.
[2] Eckardt, D., 1986, "Advanced Experimental Techniques for Turbomachinery Development," *Advanced Experimental Techniques in Turbomachinery*, D. Japikse, ed., Concepts ETI, Norwich, VT, pp. 1–52.
[3] Lucia, M., Mengoni, C., and Boncinelli, P., 2000, "Synchronized LDV Measurement in Centrifugal Impeller: Seeding Insemination Set Up and CFD Comparison," ASME Turbo Expo, Munich, Germany, May 8–11, pp. 1–7.
[4] Buffaz, N., and Trébinjac, I., 2012, "Detailed Analysis of the Flow in the Inducer of a Transonic Centrifugal Compressor," J. Therm. Sci., **21**(1), pp. 1–12.
[5] Bourgeois, J., Martinuzzi, R., Savory, E., Zhang, C., and Roberts, D., 2009, "Experimental and Numerical Investigation of an Aero-Engine Centrifugal Compressor," ASME Turbo Expo, Orlando, FL, June 8–12, pp. 1–10.
[6] Ibaraki, S., Matsuo, T., Kuma, H., Sumida, K., and Suita, T., 2003, "Aerodynamics of a Transonic Centrifugal Compressor Impeller," ASME J. Turbomach., **125**(2), pp. 346–351.
[7] Yeh, Y., and Cummins, H. Z., 1964, "Localized Fluid Flow Measurements With an HeNe Laser Spectrometer," Appl. Phys. Lett., **4**(10), pp. 176–178.
[8] Fagan, J., and Fleeter, S., 1989, "L2F and LDV Velocity Measurement and Analysis of the 3D Flow Field in a Centrifugal Compressor," Joint Propulsion Conference, Monterrey, CA, July 10–12, pp. 1–9.
[9] Jensen, K., 2004, "Flow Measurements," J. Brazilian Soc. Mech. Sci. Eng., **26**(4), pp. 400–419.
[10] Eckardt, D., 1978, *Investigation of the Jet-Wake Flow of a Highly-Loaded Centrifugal Compressor Impeller*, NASA, Washington DC.
[11] Eckardt, D., 1976, "Detailed Flow Investigations Within a High-Speed Centrifugal Compressor Impeller," ASME J. Fluids Eng., **98**(3), pp. 390–399.
[12] Krain, H., 1981, "A Study on Centrifugal Impeller and Diffuser Flow," J. Eng. Power, **103**(4), pp. 688–697.
[13] Krain, H., 1988, "Swirling Impeller Flow," ASME J. Turbomach., **110**(1), pp. 122–128.
[14] Adler, D., and Levy, Y., 1979, "Laser-Doppler Investigation of the Flow Inside a Backswept, Closed, Centrifugal Impeller," J. Mech. Eng. Sci., **21**(1), pp. 1–6.
[15] Fagan, J., and Fleeter, S., 1990, *An Investigation of the Three-Dimensional Flow Field in a Centrifugal Compressor, TR-90-C-004*, NASA, Washington, DC.
[16] Hathaway, M., Chriss, R., Wood, J. R., and Strazisar, A., 1993, "Experimental and Computational Investigation of the NASA Low-Speed Centrifugal Compressor Flow Field," ASME J. Turbomach., **115**(3), pp. 527–541.
[17] Skoch, G. J., Prahst, P., Wernet, M., Wood, J. R., and Strazisar, A., 1997, *Laser Anemometer Measurements of the Flow Field in a 4:1 Pressure Ratio Centrifugal Impeller*, NASA, Washington DC.
[18] Stahlecker, D., and Gyarmathy, G., 1998, "Investigations of Turbulent Flow in a Centrifugal Compressor Vaned Diffuser by 3-Component Laser Velocimetry," International Gas Turbine & Aeroengine Congress & Exhibition, Stockholm, Sweden, June 2–5, pp. 1–14.
[19] Stahlecker, D., Casartelli, E., and Gyarmathy, G., 1998, "Secondary Flow Field Measurements with a LDV in the Vaned Diffuser of a High-Subsonic Centrifugal Compressor," 9th International Symposium on Applications of Laser Techniques to Fluid Mechanics, Lisbon, Portugal, July 13–16, pp. 1–12.
[20] Schleer, M., and Abhari, R. S., 2008, "Clearance Effects on the Evolution of the Flow in the Vaneless Diffuser of a Centrifugal Compressor at Part Load Condition," ASME J. Turbomach., **130**(3), p. 031009.
[21] Methel, C. J., Gooding, W. J., Fabian, J. C., Key, N. L., and Whitlock, M., 2016, "The Development of a Low Specific Speed Centrifugal Compressor Research Facility," ASME Turbo Expo, Seoul, South Korea, June 13–17, ASME, pp. 1–11.
[22] Gooding, W. J., and Key, N. L., 2019, "Leveraging LDV Techniques for the Investigation of Unsteady Turbomachinery Flows," Aeronaut. J., **123**(1270), pp. 1919–1937.
[23] Orloff, K., and Snyder, P., 1982, "Laser Doppler Anemometer Measurements Using Nonorthogonal Velocity Components: Error Estimates," Appl. Opt., **21**(2), pp. 339–344.
[24] Ahmed, N., and Elder, R. L., 2000, "Flow Behaviour in a High Speed Centrifugal Impeller Passage Under 'Design' and 'Off Design' Operating Conditions," JSME Int. J., **43**(1), pp. 22–28.